Thermoelectric properties and transport mechanism of $Cu_{0.5}In_{0.5}Cr_2Se_4$ and its Zn-doped samples

Xuemin Bai[1], Yuqing Sun[1], Fang Yu[1], Jian Liu[1,*], Lanling Zhao[1], Chun-ming Wang[1, 3], Ruomeng Huang[2, *], Shengqing Xia[3], Jichao Li[1]

[1] School of Physics, Shandong University, Jinan, Shandong 250100, China

[2] School of Electronics and Computer Science, University of Southampton, Southampton, SO17 1BJ, United Kingdom

[3] State Key Laboratory of Crystal Materials, Institute of Crystal Materials, Shandong University, Jinan, Shandong 250100, China

Abstract

The thermoelectric properties and transport mechanism of $Cu_{0.5}In_{0.5}Cr_2Se_4$ and its Zn-doped samples were studied. In the middle and low temperature range, the electrical resistivity of $Cu_{0.5}In_{0.5}Cr_2Se_4$ decreases and Seebeck coefficient increases with the increase of temperature, indicating the fixed range hopping behavior of Anderson's localization. Two abnormal declines emerge simultaneously in resistivity and Seebeck coefficient at high temperatures, indicating a band regulation by temperature. After slight Zn-doping, the carrier concentration decreases slightly and the carrier mobility increases obviously, realizing electron delocalization. Both of resistivity and Seebeck coefficient decrease with further increasing Zn doping content due to the enhanced carrier concentration, resulting in the improved power factor. The thermal conductivity is extremely low in the pristine $Cu_{0.5}In_{0.5}Cr_2Se_4$ and increases with increasing Zn-doping. Due to the significant enlargement of power factor and relatively weak increase of thermal conductivity, the *ZT* value is enhanced by Zn doping from 0.30 of the pristine sample to 0.40 for the sample with 3.5% Zn doping at 773 K. Moreover, a factor of about 60% improvement of the average *ZT* is reported on the Zn-doped $Cu_{0.5}In_{0.5}Cr_2Se_4$ sample, reaching 0.26 over the temperature range between 323 K and 773 K.

[*] Corresponding author. Email address: liujjx@sdu.edu.cn (Jian Liu), r.huang@soton.ac.uk (Ruomeng Huang)

Keyword: thermoelectric materials; spinel; electrical transport; electronic localization

Introduction

Thermoelectric (TE) materials involve the ability of direct conversion between heat energy and electric energy. The performance of TE materials is characterized by the non-dimensional thermoelectric figure of merit ZT ($ZT= S^2\sigma T/\kappa$, where S is the Seebeck coefficient, σ is the electrical conductivity, T is the absolute temperature and κ is the thermal conductivity). The term $S^2\sigma$ in the numerator is also referred as the power factor (PF) which characterizes the electrical performance of the TE materials. A high PF and a low κ are essential requirements for a high ZT. TE materials with excellent electrical performance require a large effective mass of density of states (m^*_{DOS}) and a high carrier mobility [1]. m^*_{DOS} is determined by both the effective mass and the degeneracy of the bands. Energy band degeneracy includes orbital degeneracy where multiple energy bands with minimal energy difference occur convergence and valley degeneracy of multiple carrier valley pockets caused by crystal structure symmetry [2, 3]. Herein, the effective mass of the bands couples with the carrier mobility and a large band effective mass can lead to a low carrier mobility which deteriorates TE performance. Therefore, it is an attractive optimization strategy to improvement of m^*_{DOS} by increasing the band degeneracy without affecting the band effective mass and carrier mobility, which has been achieved in PbX (X = S, Se, Te) [4, 5], Mg_2X (X = Si, Sn) [6, 7] and half-Heusler (HH) alloys [8], etc. The high energy band degeneracy of these materials is fundamentally contributed by the face-centered cubic crystal structure. Moreover, orbital degeneracy can be improved by alloying or changing temperature to converge different energy bands, realizing higher thermoelectric performance [5, 9-12].

The spinel-structure materials exhibit a face-centered cubic structure with the lattice constants of about 10 Å. The general formula is AM_2X_4 [13] where A is Fe, Zn, Cd, Cu, Ni, etc, M is Cr, Co, Ti, In, Mn, etc, and X is a chalcogen element, [14-21]. When A-site is Cu, the pristine Cu-based spinel materials exhibit metallic behaviors because the valence of Cu is +1 in these materials [13, 14, 17, 22]. For instant, $CuCr_2Se_4$ is regarded

as a typical metallic spinel material. However, it exhibits a semiconducting behavior after 50% indium doping at A site ($Cu_{0.5}In_{0.5}Cr_2Se_4$) [13, 23, 24].

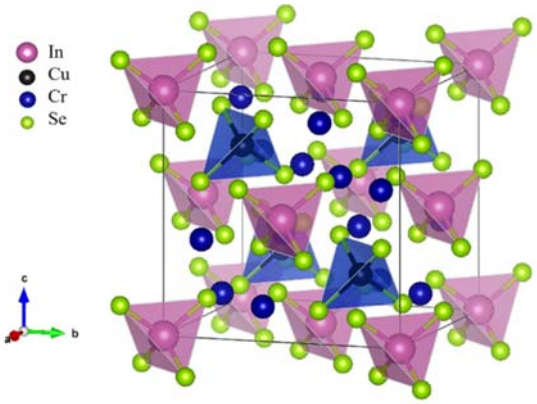

Fig. 1 Schematic representation of the crystal structures for $Cu_{0.5}In_{0.5}Cr_2Se_4$.

Spinel-structured $Cu_{0.5}In_{0.5}Cr_2Se_4$ is a p-type semiconductor with the space group $F\bar{4}3m$ as shown in Fig. 1. Due to their different ion radii and charge numbers, Cu ions and In ions occupy two different tetrahedral 4*a* and 4*d* positions while Cr ions are located at the octahedral 16*e* positions. The arrangement and distribution of atoms make the distances from Cu and In to Se unequal (i.e. 2.434 Å and 2.537 Å, respectively) [24]. It means that the $CrSe_6$ octahedrons arise lattice distortion which might contribute to a low lattice thermal conductivity. In addition, theoretical calculations show that the maximum of valence band (VBM) of $Cu_{0.5}In_{0.5}Cr_2Se_4$ has a high orbital degeneracy [22, 25]. Meanwhile, the face-centered cubic structure would also result in high energy valley degeneracy. Therefore, p-type doped $Cu_{0.5}In_{0.5}Cr_2Se_4$ may obtain higher band degeneracy. The expected low lattice thermal conductivity and high energy band degeneracy both suggest good thermoelectric performance for $Cu_{0.5}In_{0.5}Cr_2Se_4$. At present, there are few studies [13, 24] on the thermoelectric properties of $Cu_{0.5}In_{0.5}Cr_2Se_4$ and the transport mechanism remains to be further understood. In this paper, the thermoelectric properties and transport mechanism of $Cu_{0.5}In_{0.5}Cr_2Se_4$ and its Zn-doped samples were studied.

Methods

$Cu_{0.5}In_{0.5-x}Zn_xCr_2Se_4$ (x=0, 0.005, 0.015, 0.025 and 0.035) samples were prepared by the melt annealing method. Cu (99.9%), In (99.99%), Cr (99.95%) and Se (99.999%) were weighed according to the stoichiometric ratio and put into a quartz tube. Then, the quartz tube containing raw materials was evacuated and sealed. The raw materials in the quartz tube reacted at 1373 K for 10 hours to form a mixture of intermediate products and final products. The alloy ingot was fine ground and then put into the quartz tube for annealing in vacuum at 1073 K for 48 hours. The obtained powder was put into the mould for spark plasma sintering (SPS) at 1023 K for 5 minutes and under a pressure of 60 MPa, and disc samples with a diameter of about 12.7 mm and thickness of about 2 mm were obtained.

The phase structures of the powder were investigated by X-ray diffraction (XRD) with Cu $K\alpha 1$ radiation from 10 ° to 80 ° in a high-resolution diffraction system of Smartlab3KW. The microstructure and element distribution of the cross-section surface of the samples were characterized by scanning electron microscopy (SEM) and energy dispersive X-ray spectroscopy (EDS), respectively, using a Helios G4 UC instrument. The Seebeck coefficient (S) and resistivity (ρ) of 2 × 2 × 10 mm^3 bars were measured by the LSR-3/1100 instrument in a helium atmosphere when the test temperature is higher than 323 K, and the Seebeck coefficient was calculated by the differential method, obtained as the slope of linear fitting of a series of voltages due to different temperature gradients. The systematical uncertainties of the measurements of both S and ρ are about 5%. A self-made low-temperature test instrument in vacuum was used to measure the Seebeck coefficient and resistivity of 0.5 × 2 × 10 mm^3 bar based on the inversion method whose uncertainty is less than 1% [26] when the test temperature range is from 150 K to 360 K. The thermal conductivity (κ) of samples is calculated by the following formula [27]:

$$\kappa = DC_V\alpha$$

where D, C_V, α are the thermal diffusivity, specific heat capacity and sample actual density. The thermal diffusivity D of the samples were measured on the TA DLF1200 instrument through the pulsed laser transient heat flow method in nitrogen with an

uncertainty of about 3%. The specific heat capacity of the pristine sample was measured on TA DSC2500 by the 3-step method. It is found that the variation of specific heat capacity with temperature is small for three measurements as shown in Fig. S1. Because that dopants with a small content have little influence on specific heat capacity, an average value of 250 $Jkg^{-1}K^{-1}$ is used for all samples. The Hall measurements for 4 × 4 mm^2 square pellets were performed by the MMR K2500 Hall effect test system with a ±1.4 T magnetic field based on Van der Pauw method with an uncertainty of about 5%. All samples were polished to ensure that the surfaces were parallel and gilded at the four corners. The measured Hall coefficients at room temperature are listed in Table S1.

Results and discussion

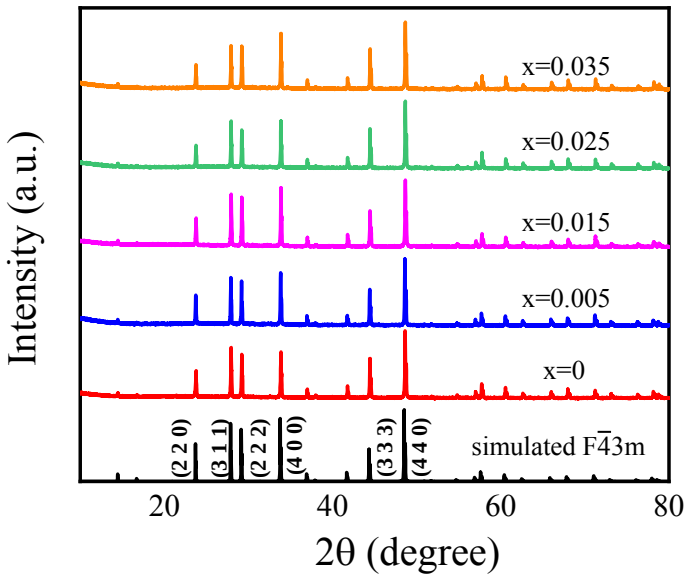

Fig. 2 Powder X-ray diffraction patterns for $Cu_{0.5}In_{0.5-x}Zn_xCr_2Se_4$ (x=0, 0.005, 0.015, 0.025 and 0.035) alloys samples at room temperature.

Fig. 2 shows the XRD of synthesized $Cu_{0.5}In_{0.5}Cr_2Se_4$ and its Zn-doped samples in the range from 10 º to 80 º. It shows that there is no obvious impurity peak as compared with the simulated diffraction peak of F$\bar{4}$3m $Cu_{0.5}In_{0.5}Cr_2Se_4$. Meanwhile, the slight upturn at small angles indicates the existence of some amorphous components. The

lattice constant of the sample was calculated by the cell refinement in jade 6.5. The lattice constants, theoretical densities and relative densities of the samples are calculated and listed in Table 1. After slightly doping Zn at In site, the lattice constant of the sample increases probably related to the suppression of the generation of vacancies as discussed below. The lattice constant of the Zn-doped samples decreases with the further increase of Zn doping, because the atomic radius of Zn is smaller than that of In. The relative densities are calculated to be about 92%. And the SEM images (Fig. S2) and EDS mapping images (Fig. S3) show the high quality of the samples.

Table 1

Lattice constant (a=b=c), theoretical density (α_{th}), actual density (α_a) and relative density (α_r) of $Cu_{0.5}In_{0.5-x}Zn_xCr_2Se_4$ (x=0, 0.005, 0.015, 0.025, 0.035) samples.

	a=b=c (Å)	α_{th} (g/cm^3)	α_a (g/cm^3)	α_r
x=0	10.582	5.71	5.25	91.9%
x=0.005	10.588	5.69	5.24	92.1%
x=0.015	10.578	5.70	5.22	91.6%
x=0.025	10.577	5.70	5.31	93.2%
x=0.035	10.576	5.70	5.25	92.1%

The temperature dependence of the resistivity and Seebeck coefficient of $Cu_{0.5}In_{0.5}Cr_2Se_4$ sample from 150 K to 773 K is shown in Fig. 3. Seebeck coefficient exhibits positive values indicating the hole-type transport properties. With increasing temperature, the resistivity decreases exhibiting a semiconducting behavior, however, Seebeck coefficient increases exhibiting a degenerated semiconductor behavior. The carrier concentration was measured to be about 1×10^{20} cm^{-3} at room temperature which is relatively large as compared with those of some state-of-art pristine TE materials [28-30]. Such a large carrier concentration indicates a large amount of intrinsic defects in pristine $Cu_{0.5}In_{0.5}Cr_2Se_4$, consistent with the results reported in the

single crystal [24], and should result in the degenerated semiconductor behaviors which is consistent with the measured Seebeck coefficient. Furthermore, the magnitude of Seebeck coefficient of $Cu_{0.5}In_{0.5}Cr_2Se_4$ is much larger than those of other TE materials with the same carrier concentration [31, 32], which implies a high degeneracy of the energy band near VBM and/or a very large effective mass.

Therefore, the semiconducting behavior of resistivity could be probably attributed to the electronic localization (so called Anderson localization). Lattice disorder induced by intrinsic defects might scatter the carriers, and cause the carriers near valence band maximum localized. And the heavier the effective mass is, the stronger effects the disordered structures exert on the carriers. Strong electronic localization and semiconducting behavior in resistivity indicate the heavy effective mass of carriers in $Cu_{0.5}In_{0.5}Cr_2Se_4$. According to the Anderson localization theory, in a disordered system, the Fermi level (E_F) locates in the localized states and most of carriers are localized at low temperatures and do not contribute to electrical conductance [33]. When temperature increases, the carriers in the localized states are activated and jump into the itinerant states. This leads to the increase number of the effective carriers, resulting in the semiconducting resistivity. This behavior is the so-called thermal-activated fixed-range hopping behavior, and the resistivity is described as the following equation [33]:

$$\rho(T) = \rho_0 exp(\Delta E/k_B T)$$

where ρ_0 is a constant, ΔE is the thermal activation energy which is generally much smaller than the intrinsic band gap, k_B is the Boltzmann constant and T is the absolute temperature, respectively. The temperature dependence of resistivity of $Cu_{0.5}In_{0.5}Cr_2Se_4$ obeys this equation very well in the temperature region between 186 K and 368 K, as fitted and shown in Fig. 3(a). The thermal activation energy is fitted to be about 0.04 eV, which is far less than the energy band gap of $Cu_{0.5}In_{0.5}Cr_2Se_4$. Therefore, in the temperature range of 186 K ~ 368 K, the thermal activation of $Cu_{0.5}In_{0.5}Cr_2Se_4$ sample is the Anderson localization behavior rather than that of intrinsic semiconductor. Generally, a localized system would exhibit the variable-range hopping behavior in the lower temperature region, however, the resistivity of $Cu_{0.5}In_{0.5}Cr_2Se_4$ does not follow

this behavior below 186 K because of its magnetic transition at lower temperatures as reported in the literature [24].

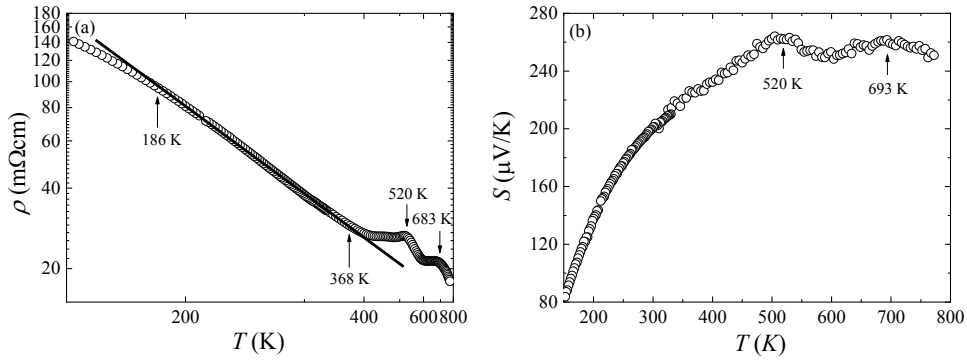

Fig. 3 Temperature dependence of the (a) electrical resistivity, (b) Seebeck coefficient for $Cu_{0.5}In_{0.5}Cr_2Se_4$. Black solid line represents variation curve of $\ln\rho$ and T^{-1}.

Notably, as temperature increases up to about 520 K and 690 K, both of the resistivity and Seebeck coefficient decrease and show an abnormal temperature dependence. The simultaneous changes indicate a band structure phenomenon. Considering the complex band structure of valence bands of $Cu_{0.5}In_{0.5}Cr_2Se_4$, the bands in the deep valence band might contribute to the electrical transport when the temperature is high enough. Similar results were reported in the literature [34]. However, the detailed mechanism still calls for further investigation.

Electron localization hinders the electrical transport and reduces the electrical conductivity and inhibits the thermoelectric performance of materials. Element doping is a common strategy to tailor electronic structure and regulate thermoelectric properties. Therefore, the effects of Zn doping at the In site on the thermoelectric properties of $Cu_{0.5}In_{0.5}Cr_2Se_4$ were studied.

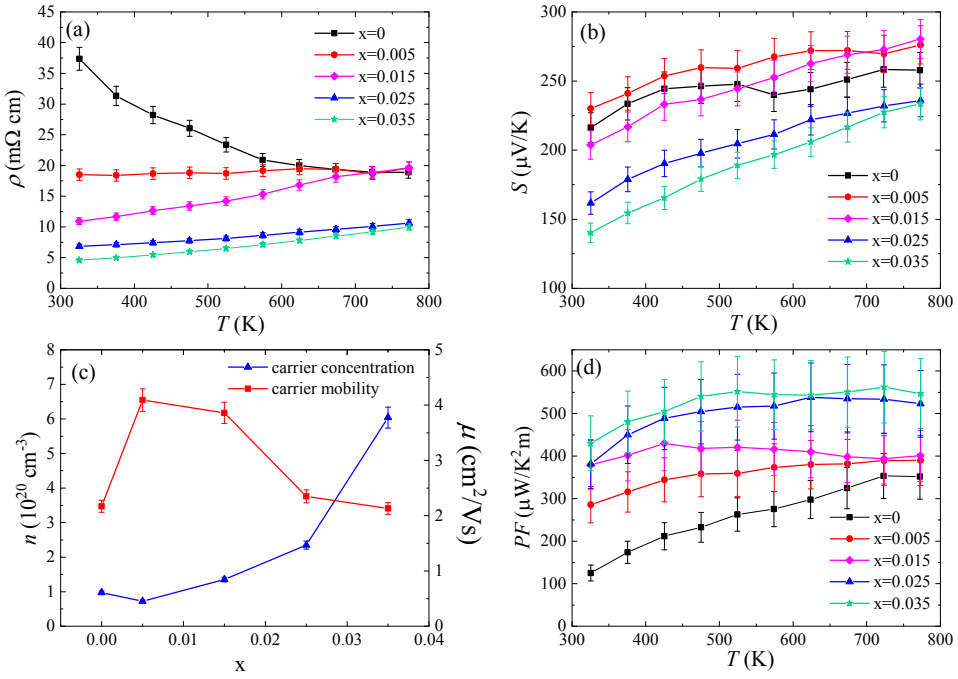

Fig. 4 Temperature dependence of (a) electrical resistivity and (b) Seebeck coefficient for $Cu_{0.5}In_{0.5-x}Zn_xCr_2Se_4$(x=0, 0.005, 0.015, 0.025, 0.035). (c) Carrier concentration and mobility at room temperature of $Cu_{0.5}In_{0.5-x}Zn_xCr_2Se_4$(x=0, 0.005, 0.015, 0.025, 0.035) materials as functions of doping content. (d) Temperature dependence of *PF* for $Cu_{0.5}In_{0.5-x}Zn_xCr_2Se_4$(x=0, 0.005, 0.015, 0.025, 0.035).

The temperature dependences of resistivity and Seebeck coefficient of $Cu_{0.5}In_{0.5-x}Zn_xCr_2Se_4$ (x = 0, 0.005, 0.015, 0.025, 0.035) samples are shown in Fig. 4. A slight Zn doping (x = 0.005) significantly reduced the room temperature resistivity and resulted in a weak temperature dependence in the whole measured temperature range. Concurrently, an increase in the Seebeck coefficient was also observed as shown in Fig. 4(b). According to the results of Hall measurements at room temperature (Fig. 4(c)), the carrier concentration decreases slightly when 0.5% Zn is doped, which is consistent with the enhanced Seebeck coefficient. Meanwhile, the significant increase in the carrier mobility is the dominating contribution to the reduction of the resistivity near room temperature. It is preliminarily determined that Zn doping realizes electronic

delocalization and is probably related to the suppression of intrinsic defects. The small amount doping of Zn at In sites inhibits the emergence of intrinsic defects, which leads to decrease of the carrier concentration and the increase of the carrier mobility of the 0.5% Zn-doped sample. When Zn doping content further increases, both of the resistivity and Seebeck coefficient decrease due to the significant increase of carrier concentration, and their temperature dependences exhibit the degenerated semiconducting behaviors. Therefore, the electrical transport of doped samples no longer shows the Anderson localization phenomenon and electronic delocalization is realized by Zn doping. It should be noted that the abnormal behavior at high temperatures is weakened and vanished as Zn doping content increases. These changes of resistivity and Seebeck coefficient with Zn doping indicate a modulation on the band structure. Benefited from the significant reduced resistivity, the power factor increases obviously in the whole temperature region measured and the maximum value increases from 350 μW/K^{2}m of the pristine sample to 550 μW/K^{2}m of the sample of x = 0.035. The maximum *PF* value in this work is similar with that of isotypic $Cu_{0.47}Ga_{0.53}Cr_2Se_4$ in the literature (560 μW/K^{2}m) [13].

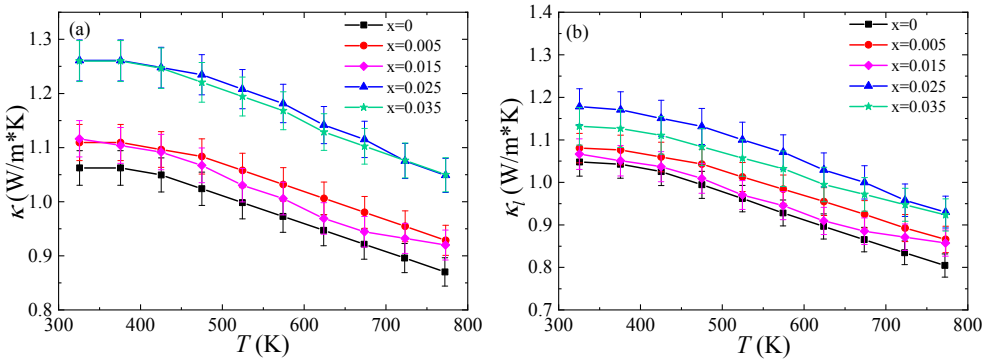

Fig. 5 Temperature dependence of (a) thermal conductivity and (b) lattice thermal conductivity for $Cu_{0.5}In_{0.5-x}Zn_xCr_2Se_4$ (x = 0, 0.005, 0.015, 0.025, 0.035)

The total thermal conductivity of $Cu_{0.5}In_{0.5-x}Zn_xCr_2Se_4$ (x = 0, 0.005, 0.015, 0.025, 0.035) samples decreases with the increase of temperature as shown in Fig. 5(a). The thermal conductivity of pristine sample varies from 1.1 Wm^{-1}K^{-1}at room temperature

to 0.88 $Wm^{-1}K^{-1}$ at 773 K, which is comparable with those of the state-of-art TE materials [35-37]. However, the thermal conductivity increases with the increase of doping content. According to Wiedemann-Franz Law, the electronic thermal conductivity was calculated and shown in Fig. S6, where the Lorentz number (L) was calculated from Seebeck coefficient based on the formula [38]:

$$L = 1.5 + \exp(-|S|/116)$$

The electronic thermal conductivity is enhanced by Zn doping because of the significantly reduced electrical resistivity. After subtracting the electronic thermal conductivity from the total thermal conductivity, the lattice thermal conductivity is calculated and shown in Figure 5(b). The lattice thermal conductivity decreases with increasing temperature due to the phonon U-process scattering, and contributes dominantly to the total thermal conductivity. The magnitude of lattice thermal conductivity increases after Zn doping as compared with that of pristine sample. This is probably attributed to the suppression of intrinsic defects as considering the electron delocalization. The suppression of intrinsic defects weakens phonon scattering, resulting to increase of lattice thermal conductivity after doping Zn. However, it was found that lattice thermal conductivity of Zn-doped samples varies non-monotonically with the doping amount of Zn, which might related to the non-monotonic relative density.

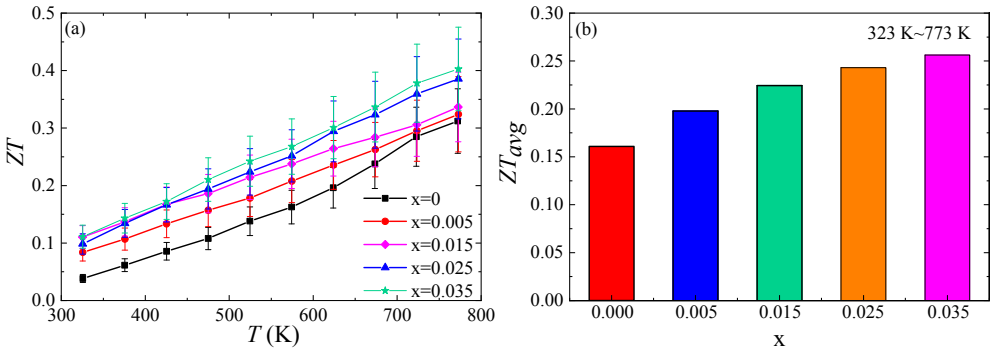

Fig. 6 (a) Temperature dependence of figure of merit ZT, (b) average ZT value for $Cu_{0.5}In_{0.5-x}Zn_xCr_2Se_4$ (x = 0, 0.005, 0.015, 0.025, 0.035)

Fig. 6(a) shows the temperature dependence of figure of merit *ZT* for $Cu_{0.5}In_{0.5-x}Zn_xCr_2Se_4$ (x = 0, 0.005, 0.015, 0.025, 0.035) samples. The *ZT* values of all samples increases monotonically with the increase of temperature. The *ZT* value of pristine $Cu_{0.5}In_{0.5}Cr_2Se_4$ sample reaches a maximum of about 0.30 at 773 K. Although the thermal conductivity increases after Zn doping because of the enhancement of both electronic and lattice components, the enhanced power factor plays the predominant role on the figure of merit. The figure of merit is enhanced by Zn doping in the whole temperature region measured, and reaches the maximum ~ 0.40 at 773 K in the x=0.035 sample, which is more than two times higher than the reference data reported for $Cu_{0.47}Ga_{0.53}Cr_2Se_4$ (0.17) [13]. The average *ZT* values (ZT_{avg}) of samples from 323 K to 773 K are shown in Fig .6(b). The ZT_{avg} is calculated by the following formula [39]:

$$ZT_{avg} = \frac{1}{T_h - T_c}\int_{T_c}^{T_h} ZT\,d\,T$$

where T_h and T_c are the upper and lower limits of temperature range. The ZT_{avg} of Zn-doped samples increases monotonically with the increase of Zn doping. The x=0.035 alloy shows the highest ZT_{avg} ~ 0.26, which improved by a factor of 60% as compared with the pristine sample. These results show that $Cu_{0.5}In_{0.5}Cr_2Se_4$ is a promising thermoelectric materials, and its TE performance might be further improved by preferable modulation on electrical properties.

Conclusion

In this paper, we studied the thermoelectric properties and transport mechanism of $Cu_{0.5}In_{0.5}Cr_2Se_4$ and its doped samples. The pristine $Cu_{0.5}In_{0.5}Cr_2Se_4$ sample demonstrates the fixed range hopping Anderson localization behavior in the low and middle temperature ranges. Two abnormal declines emerge simultaneously in resistivity and Seebeck coefficient at about 520 K and 690 K, indicating a band regulation by temperature. When lightly doped with Zn at In site, the hole concentration decreases slightly and the carrier mobility increases obviously, indicating electronic delocalization. With further increase of Zn doping, the magnitude of resistivity and Seebeck coefficient decrease because of the increase of hole concentration, resulting in

the obviously improved power factor. The total thermal conductivity increases after Zn doping due to the increase of both electronic and lattice components. The figure of merit *ZT* is enhanced by Zn doping due to the remarkable improvement of power factor, reaching a maximum of 0.40 in the $Cu_{0.5}In_{0.465}Zn_{0.035}Cr_2Se_4$ sample. Correspondingly, the average *ZT* is enhanced by a factor of 60%, from 0.16 to 0.26.

Acknowledgements

This work was supported by the National Science Foundation of Shandong Province, China (Grant No. ZR2018MEM015), National Natural Science Foundation of China (Grant No. 51872166), Shandong Provincial Natural Science Foundation-Quantum Science Research Joint fund (Grant No. ZR2020LLZ006), Shandong University Seed Fund Program for International Research Cooperation, the Fundamental Research Funds for the Central Universities and EPSRC IAA funding.

Supporting Information

The Supporting Information is available free of charge at

Specific heat capacity, SEM, EDS, Repeat measurements of resistivity and Seebeck coefficient, Lorentz number calculated from Seebeck coefficient, Electronic thermal conductivity, Hall coefficient, effective mass, Lorentz number calculated based on SPB mode and detailed description of electrical transport of Anderson localization.

References

[1] G. Tan, L. Zhao, M. G. Kanatzidis, Rationally designing high-performance bulk thermoelectric materials, Chem. Rev., 116 (2016), 12123-12149. https://doi.org/10.1021/acs.chemrev.6b00255.

[2] T. Zhu, Y. Liu, C. Fu, J. P. Heremans, J. G. Snyder, X. Zhao, Compromise and synergy in high-efficiency thermoelectric materials, Adv. Mater., 29 (2017), 1605884. https://doi.org/10.1002/adma.201605884.

[3] Y. Pei, H. Wang, G. J. Snyder, Band engineering of thermoelectric materials, Adv. Mater., 24 (2012), 6125-6135. https://doi.org/10.1002/adma.201202919.

[4] C. M. Jaworski, M. D. Nielsen, H. Wang, S. N. Girard, W. Cai, W. D. Porter, M. G. Kanatzidis, J. P. Heremans, Valence-band structure of highly efficient p-type thermoelectric PbTe-PbS alloys, Phys. Rev. B, 87 (2013), 045203. https://doi.org/10.1103/PhysRevB.87.045203.

[5] Y. Pei, X. Shi, A. LaLonde, H. Wang, L. Chen, G. J. Snyder. Convergence of electronic bands for high performance bulk thermoelectrics, Nature, 473 (2011), 66-69. https://doi.org/10.1038/nature09996.

[6] W. Liu, X. Tan, K. Yin, H. Liu, X. Tang, J. Shi, Q. Zhang, C. Uher, Convergence of conduction bands as a means of enhancing thermoelectric performance of n-type $Mg_2Si_{1-x}Sn_x$ solid solutions, Phys. Rev. Lett., 108 (2012), 166601. https://doi.org/10.1103/PhysRevLett.108.166601.

[7] X. Liu, T Zhu, H. Wang, L. Hu, H. Xie, G. Jiang, G. J. Snyder, X. Zhao, Low electron scattering potentials in high performance $Mg_2Si_{0.45}Sn_{0.55}$ based thermoelectric solid solutions with band convergence, Adv. Energy Mater., 3 (2013), 1238-1244. https://doi.org/10.1002/aenm.201300174.

[8] M. Lee, F. P. Poudeu, S. D. Mahanti, Electronic structure and thermoelectric properties of Sb-based semiconducting half-Heusler compounds, Phys. Rev. B, 83 (2011), 159907. https://doi.org/10.1103/PhysRevB.83.085204.

[9] H. Wang, Z. M. Gibbs, Y. Takagiwa, G. J. Snyder, Tuning bands of PbSe for better thermoelectric efficiency, Energy Environ. Sci., 7 (2014), 804-811. https://doi.org/10.1039/C3EE43438A.

[10] P. Jood, J. P. Male, S. Anand, Y. Matsushita, Y. Takagiwa, M. G. Kanatzidis, G. J. Snyder, M. Ohta, Na Doping in PbTe: Solubility, band convergence, phase boundary mapping, and thermoelectric properties, J. Am. Chem. Soc., 142 (2020), 15464-15475.

https://doi.org/10.1021/jacs.0c07067.

[11] C. Fu, T. Zhu, Y. Liu, H. Xie, X. Zhao, Band engineering of high performance p-type FeNbSb based half-Heusler thermoelectric materials for figure of merit zT > 1, Energy Environ. Sci., 8 (2015), 216-220. https://doi.org/10.1039/C4EE03042G.

[12] J. Gainza, F. Serrano-Sánchez, J. E. Rodrigues, J. Prado-Gonjal, N. M. Nemes, N. Biskup, O. J. Dura, J. L. Martínez, F. Fauth, J. A. Alonso, Unveiling the correlation between the crystalline structure of M-filled $CoSb_3$ (M = Y, K, Sr) skutterudites and their thermoelectric transport properties. Adv. Funct. Mater., 30 (2020), 2001651. https://doi.org/10.1002/adfm.202001651.

[13] G. J. Snyder, T. Caillat, J. P. Fleurial, Thermoelectric properties of chalcogenides with the spinel structure, Mater. Res. Innov., 5 (2001), 67-73. https://doi.org/10.1007/s100190100133.

[14] K. Hashikuni, K. Suekuni, H. Usui, R. Chetty, Mi. Ohta, K. Kuroki, T. Takabatake, K. Watanabe, M. Ohtaki, Thermoelectric properties and electronic structures of $CuTi_2S_4$ thiospinel and its derivatives: structural design for spinel-related thermoelectric materials, Inorg. Chem., 58 (2019), 1425-1432. https://doi.org/10.1021/acs.inorgchem.8b02955.

[15] M. Ito, T. Yamashita, S. Ebisu, S. Nagata, Thermodynamic and electrical properties of $CuCrTiS_4$, J. Alloys Compd., 598 (2014), 133-136. https://doi.org/10.1016/j.jallcom.2014.01.222.

[16] J. Dinger, T. Reimann, E. Ovodok, J. Töpfer, Cation distribution in $NiMn_2O_4$ spinel probed by high temperature thermopower measurements, J. Alloys Compd., 865 (2021), 158909. https://doi.org/10.1016/j.jallcom.2021.158909.

[17]E. Maciążek, E. Malicka, A. Gągor, Z. Stokłosa, T. Groń, B. Sawicki, H. Duda, A. Gudwański, Semiconducting-metallic transition of singlecrystalline ferromagnetic Hf-doped $CuCr_2Se_4$ spinels, Physica B, 520 (2017), 116-122. https://doi.org/10.1016/j.physb.2017.05.049.

[18] P. Wyżga, I. Veremchuk, P. Koželj, A. Leithe-Jasper, R. Gumeniuk, Mn-for-Fe substitution in $Fe_{1-x}Mn_xIn_2S_4$ thiospinel - Crystal structure and thermoelectric properties, J. Phys. Chem. Solids, 152 (2021), 109984. https://doi.org/10.1016/j.jpcs.2021.109984.

[19] Y. Lang, L. Pan, C. Chen, Y. Wang, Thermoelectric properties of thiospinel-type $CuCo_2S_4$, J. Electron. Mater., 48 (2019), 4179-4187. https://doi.org/10.1007/s11664-019-07182-x.

[20] J. Hemberger, P. Lunkenheimer, R. Fichtl, H. A. Krug von Nidda, V. Tsurkan ,A. Loidl, Relaxor ferroelectricity and colossal magnetocapacitive coupling in ferromagnetic $CdCr_2S_4$. Nature, 434

(2005), 364-367. https://doi.org/10.1038/nature03348.

[21] W. S. Seo, R. Otsuka, H. Okuno, M. Ohta, K. Koumoto, Thermoelectric properties of sintered polycrystalline $ZnIn_2S_4$. J. Mater. Res., 14 (1999), 4176-4181. https://doi.org/10.1557/JMR.1999.0565.

[22] A. U. Khan, R. A. R. A. Orabi, A. Pakdel, J. Vaney, B. Fontaine, R. Gautier, J. Halet, S. Mitani, T. Mori, Sb doping of metallic $CuCr_2S_4$ as a route to highly improved thermoelectric properties, Chem. Mater., 29 (2017), 2988-2996. https://doi.org/10.1021/acs.chemmater.6b05344.

[23] E. Maciążek, H. Duda, T. Groń, T. Mydlarz, A. Kita, Magnetic properties of the $Cu_xIn_yCr_zSe_4$ single crystals, J. Alloys Compd., 442 (2007), 183-185. https://doi.org/10.1016/j.jallcom.2006.09.153.

[24] H. Duda, E. Maciążek, T. Groń, S. Mazur, A. W. Pacyna, A. Waśkowska, T. Mydlarz, A. Gilewski. Spin-glass-like behavior in single-crystalline $Cu_{0.44}In_{0.48}Cr_{1.95}Se_4$, Phys. Rev. B, 77 (2008), 035207. https://doi.org/10.1103/PhysRevB.77.035207.

[25] K. Ahn, M. Soroka, P. Levinský, K. Knížek, J. Hejtmánek, V. Kucek, J, Navrátil, Thermal transport in $CuCr_2X_4$ (X=S, Se, Te): Experiment and ab initio calculations, Phys. Rev. B, 104 (2021), 085146. https://doi.org/10.1103/PhysRevB.104.085146.

[26] J. Liu, Y. Zhang, Zhen Wang, M. Li, W. Su, M. Zhao, S. Huang, S. Xia, C. Wang, Accurate measurement of Seebeck coefficient, Rev. Sci. Instrum., 87 (2016), 064701. https://doi.org/10.1063/1.4952744.

[27] A. Charoenphakdee, K. Kurosaki1, H. Muta1, M. Uno1, S. Yamanaka, Ag_8SiTe_6: A new thermoelectric material with low thermal conductivity, Jpn. J. Appl. Phys. 48 (2009),011603. https://doi.org/10.1143/JJAP.48.011603.

[28] L. Zhao, J. He, D. Berardan, Y. Lin, J. Li, C. Nan, N. Dragoe, BiCuSeO oxyselenides: new promising thermoelectric materials, Energy Environ. Sci., 7 (2014), 2900-2924. https://doi.org/10.1039/C4EE00997E.

[29] M. Hong, T. C. Chasapis, Z. Chen, L. Yang, M. G. Kanatzidis, G. J. Snyder, J. Zou, n□type $Bi_2Te_{3-x}Se_x$ nanoplates with enhanced thermoelectric efficiency driven by wide-frequency phonon scatterings and synergistic carrier scatterings, ACS Nano, 10 (2016), 4719-4727. https://doi.org/10.1021/acsnano.6b01156.

[30] J. A. Grovogui, T. J. Slade, S.Hao, C. Wolverton, M. G. Kanatzidis, V. P. Dravid, Implications of doping on microstructure, processing, and thermoelectric performance: The case of PbSe, J. Mater. Res., 36 (2021), 1272-1284. https://doi.org/10.1557/s43578-021-00130-8.

[31] A. M. Dehkordi, M. Zebarjadi, J. He, T. M. Tritt, Thermoelectric power factor: enhancement mechanisms and strategies for higher performance thermoelectric materials, Mater. Sci. Eng., R 97 (2015), 1-22. https://doi.org/10.1016/j.mser.2015.08.001.

[32] Y. Pei, A. LaLonde, S. Iwanaga, G. J. Snyder, High thermoelectric figure of merit in heavy hole dominated PbTe, Energy Environ. Sci., 4 (2011), 2085-2089. https://doi.org/10.1039/C0EE00456A.

[33] N. F. Mott, E. A. Davis, Electronic Processes in Non-Crystalline Materials, second ed., Oxford University Press, New York, 1979.

[34] J. Tang, B. Gao, S. Lin, J. Li, Z. Chen, F. Xiong, W. Li, Y. Chen, Y. Pei, Manipulation of band structure and interstitial defects for improving thermoelectric SnTe, Adv. Funct. Mater., 28 (2018), 1803586. https://doi.org/10.1002/adfm.201803586.

[35] C. Gayner, K. K. Kar, Recent advances in thermoelectric materials, Prog. Mater. Sci., 83, (2016), 330-382. https://doi.org/10.1016/j.pmatsci.2016.07.002.

[36] J. Li, S. Li, Q. Wang, L. Wang, F. Liu, W. Ao, Effect of Ce-doping on thermoelectric properties in PbTe alloys prepared by spark plasma sintering, J. Electron. Mater., 40 (2011), 2063-2068. https://doi.org/10.1007/s11664-011-1715-9.

[37] X. Tang, W. Xie, H. Li, W. Zhao, Q. Zhang, M. Niino, Preparation and thermoelectric transport properties of high-performance p-type Bi_2Te_3 with layered nanostructure, Appl. Phys. Lett., 90 (2007), 012102. https://doi.org/10.1063/1.2425007.

[38] H. S. Kim, Z. M. Gibbs, Y. L. Tang, H. Wang, G. J. Snyder, Characterization of Lorenz number with Seebeck coefficient measurement, APL Mater., 3 (2015), 041506. https://doi.org/10.1063/1.4908244.

[39] L. Zhao, X. Zhang, H. Wu, G. Tan, Y. Pei, Y. Xiao, C. Chang, D. Wu, H. Chi, L. Zheng, S. Gong, C. Uher, J. He, M. G. Kanatzidis, Enhanced thermoelectric properties in the counter-doped SnTe system with strained endotaxial SrTe, J. Am. Chem. Soc., 138 (2016), 2366-2373. https://doi.org/10.1021/jacs.5b13276.